Quantitative intra-Golgi transport and organization data suggest the stable compartment nature of the Golgi

Hieng Chiong Tie[1,2], Haiyun Wang[1], Divyanshu Mahajan[1], Xiuping Sun[1], Bing Chen[1], and Lei Lu[1]

[1]School of Biological Sciences, Nanyang Technological University, Singapore

[2] Medisix Therapeutics, 11 Biopolis Way, #05-08/09 Helios, Singapore 138667

Keywords

Golgi, membrane trafficking, intra-Golgi transport, cisternal progression model, stable compartment model

*Correspondence should be addressed to:

Lei Lu (PhD)

School of Biological Sciences, Nanyang Technological University, 60 Nanyang Drive, Singapore 637551; Tel: 65-65922591; Fax: 65-67913856; Email: lulei@ntu.edu.sg

Abstract

How the intra-Golgi secretory transport works remains a mystery. The cisternal progression and the stable compartment models have been proposed and are under debate. Classic cisternal progression model posits that both the intra-Golgi transport and Golgi exit of secretory cargos should occur at a constant velocity dictated by the cisternal progression; furthermore, COPI-mediated intra-Golgi retrograde transport is essential for maintaining the Golgi organization. Leveraging our recently developed Golgi imaging tools in nocodazole-induced Golgi ministacks, we found that the intra-Golgi transport velocity of a secretory cargo decreases during their transition from the cis to the trans-side of the Golgi, and different cargos exhibit distinct velocities even within the same cisternae. We observed a vast variation in the Golgi residence times of different cargos. Remarkably, truncation of the luminal domain causes the Golgi residence time of Tac — a standard transmembrane secretory cargo without intra-Golgi recycling signals — to extend from 16 minutes to a notable 3.4 hours. Additionally, when COPI-mediated intra-Golgi retrograde transport was inhibited by brefeldin A, we found that nocodazole-induced Golgi can remain stacked for over 30 - 60 minutes. Therefore, our findings challenge the classical cisternal progression model and suggest the stable compartment nature of the Golgi.

Introduction

The Golgi complex in mammalian cells plays a crucial role in membrane trafficking and post-translational modification of proteins and lipids. Centrally positioned around the microtubule organization center(Glick and Luini, 2011; Klumperman, 2011), it comprises laterally connected Golgi stacks, each containing 4 – 7 tightly adjacent membrane sacs known as cisternae. Conventionally, a Golgi stack is recognized to have three regions: the *cis*, medial, and *trans*-Golgi. The *trans*-Golgi network (TGN) assembles outside the *trans*-side of a Golgi stack and is mainly composed of tubular and vesicular membranes(De Matteis and Luini, 2008). In the secretory pathway, newly synthesized proteins and lipids (cargos) exit the ER at the ER exit site (ERES), pass the ER and Golgi intermediate compartment (ERGIC), and reach the Golgi. Cargos subsequently transit from the *cis*-side through the medial and eventually reach the *trans*-side of the Golgi, where they exit the Golgi and target the plasma membrane(Tie et al., 2016).

Despite decades of research, the Golgi remains one of the most enigmatic organelles, particularly regarding the mechanism of intra-Golgi transport of secretory cargos(Emr et al., 2009; Glick and Luini, 2011). Two primary intra-Golgi transport models have been proposed and are currently the subject of debate. In the classic cisternal progression or maturation model, secretory cargos passively reside within Golgi cisternae, which progress or mature from the *cis* to the *trans*-Golgi cisternae to facilitate the forward or anterograde transport of cargos. Simultaneously, post-translational modification enzymes such as glycosyltransferases move in reverse or retrograde transport, altering cisternal properties to become the next cisternae of the Golgi stack. Under this perspective, the Golgi functions at a dynamic equilibrium of anterograde and retrograde intra-Golgi transport. The model predicts that all secretory cargos should have the same and constant intra-Golgi transport and Golgi exit velocity. It can provide a plausible explanation for the intra-Golgi transition of oversized secretory cargos(Bonfanti et al., 1998; Mironov et al., 2001). Moreover, direct observations of cisternal maturation have been made in budding yeast *Saccharomyces cerevisiae*(Kurokawa

et al., 2019; Losev et al., 2006; Matsuura-Tokita et al., 2006), although similar observation has not been reported in mammalian cells. However, the budding yeast Golgi differs significantly from the mammalian one in the cisternal organization – it scatters throughout the cytoplasm as unstacked compartments. This substantial difference casts doubt on the general applicability of the budding yeast Golgi observation to higher eukaryotes. In contrast, the stable compartment model posits that Golgi cisternae are stable entities. During intra-Golgi transport, carriers actively move secretory cargos from one cisterna or compartment to the next, from the *cis* to the *trans*-side, while post-translational modification enzymes remain stationary. At the *trans*-side of the Golgi, cargos are sorted into carriers bound for the plasma membrane. As a result, different cargos can exhibit distinct intra-Golgi transport and Golgi exit velocities under this model.

The ongoing debate between these two models underscores the complexity of the Golgi and reflects the insufficiency of the existing experimental data, especially the intra-Golgi transport kinetics data. Two semi-quantitative approaches exist for studying the intra-Golgi transport kinetics of ER-synchronized secretory cargos. The first is the biochemical approach, where intra-Golgi transport kinetics can be indirectly deduced by subtracting ER-to-Golgi and Golgi-to-plasma membrane transport from the overall secretion (ER-to-plasma membrane transport) during the chase. However, this indirect approach provides only an averaged intra-Golgi transport kinetics, making it incapable of measuring the instantaneous intra-Golgi transport velocity at a sub-Golgi region. The second approach involves electron microscopy (EM) imaging of immuno-gold labeled secretory cargos at Golgi cisternae(Beznoussenko et al., 2014; Trucco et al., 2004). The distribution of gold particles among individual Golgi cisternae during the chase directly indicates intra-Golgi transport kinetics. Nevertheless, this approach demands specialized techniques and equipment and considerable manual work in EM imaging and subsequent image examination, limiting its widespread use in other labs.

The limitations in current approaches call for novel methods, especially ones based on fluorescence microscopy, to resolve the intra-Golgi transport spatially and kinetically. However,

optically resolving the intra-Golgi secretory transport in mammalian cells is challenging due to the thinness (200 – 400 nm) and random orientation of Golgi stacks. To overcome this, we leverage the uniform and rotationally symmetrical arrangement of nocodazole-induced Golgi ministacks (hereafter referred to as Golgi ministacks). Extensive studies have provided strong evidence that ministacks obtained under prolonged nocodazole treatment (≥ 3 hours), the condition employed in our studies, largely represent the native Golgi stack(Cole et al., 1996; Fourriere et al., 2016; Rogalski et al., 1984; Tie et al., 2018; Trucco et al., 2004; Van De Moortele et al., 1993). We developed a numerical Golgi localization tool called Golgi localization by imaging centers of mass (GLIM) that can precisely pinpoint a Golgi protein's cisternal localization with nanometer accuracy in Golgi ministacks(Tie et al., 2017; Tie et al., 2016). Alongside this, we propose using the metric of Golgi residence time to quantify a Golgi protein's retention in the Golgi(Sun et al., 2021; Sun et al., 2020).

Here, we utilized past and newly acquired GLIM and Golgi residence time data to analyze intra-Golgi transport and Golgi exit kinetics quantitatively. Our data revealed that neither intra-Golgi transport nor Golgi exit exhibits a constant velocity. We discovered that when the luminal domain of Tac — a conventional transmembrane secretory cargo lacking intra-Golgi recycling signals — is truncated, its Golgi residence time increases from 16 min to a substantial 3.4 h. Through GLIM, we examined the cisternal organization of Golgi ministacks under brefeldin A (BFA) treatment, which halts retrograde intra-Golgi transport. Remarkably, under this condition, we found that nocodazole-induced Golgi ministacks can remain stacked for 30 - 60 min. Therefore, our findings underscore the stable nature of Golgi cisternae. They challenge the classical cisternal progression model and favor the stable compartment model.

Results and discussion

The intra-Golgi transport is not a motion with constant velocity

The classic cisternal progression model postulates that the intra-Golgi transport velocity of a secretory cargo should remain constant. However, this prediction has not been directly tested due to the inherent challenge of measuring the intra-Golgi transport velocity. The advent of GLIM has allowed us to address this issue. In GLIM, briefly, HeLa cells expressing the RUSH secretory cargo (RUSH reporter)(Boncompain et al., 2012) and GalT-mCherry, a *trans*-Golgi marker containing amino acids 1-81 of B4GALT1, were initially treated with nocodazole and cycloheximide (a protein synthesis inhibitor). Subsequently, cells were chased in biotin with nocodazole and cycloheximide for various lengths of time (*t*) before immuno-fluorescence labeling for endogenous GM130, a *cis*-Golgi marker. Except for TNFα-SBP-GFP, which uses Ii-Streptavidin as the ER hook, all RUSH reporters employ signal sequence fused streptavidin-KDEL as their ER hook. Additionally, apart from SBP-GFP, a soluble secretory protein, all RUSH reporters we selected are transmembrane proteins. We calculated centers of mass as the positions of GM130, RUSH cargo, and GalT-mCherry within each analyzable Golgi ministack. The RUSH cargo's Golgi localization quotient, or *LQ*, is calculated by dividing its distance from GM130 by GalT-mCherry's distance from GM130. The *LQ* is a linear numerical metric to indicate a cargo's axial localization within the Golgi, with a nanometer range of precision(Tie et al., 2017; Tie et al., 2016). We previously linearly defined regions of Golgi: ERES/ERGIC ($LQ < -0.25$), *cis* ($-0.25 \leq LQ < 0.25$), medial ($0.25 \leq LQ < 0.75$), *trans*-Golgi ($0.75 \leq LQ < 1.25$), and TGN ($LQ \geq 1.25$).

To analyze the intra-Golgi transport kinetics of secretory cargos, we measured the *LQ*s of RUSH reporters after various durations of biotin administration (chase). Most kinetic data was previously reported (Tie et al., 2017; Tie et al., 2016) and re-analyzed here. Additionally, we generated new data and replicated specific measurements. Figures 1, Supplementary Figure 1, and Supplementary File 1 illustrate that our *LQ* vs. time plots are highly reproducible. As previously reported, all *LQ* vs. time plots fit the following first-order exponential function

(Equation 1) well with an adjusted R^2 (adj. R^2) ≥ 0.91 (Fig. 1A-J and Supplementary Fig. 1A-M, left panels).

$$LQ = y_0 - Ae^{(-ln2\frac{t}{t_{intra}})} \qquad \text{(Equation 1)}$$

In Equation 1, t represents chase time in minutes (biotin treatment starts at t = 0); $ln2$ is the natural logarithm of 2; A is a constant; y_0 represents the LQ of the Golgi exit site; t_{intra} is the time that the cargo reaches half of the transport range and is hereafter referred to as the intra-Golgi transport time. We define the instantaneous intra-Golgi transport velocity as the derivative of LQ with respect to time, dLQ/dt, which measures the axial transport velocity of the center of the mass of the synchronized cargo wave. It should also follow the first-order exponential function (Equation 2).

$$\frac{dLQ}{dt} = ln2\frac{A}{t_{intra}}e^{(-ln2\frac{t}{t_{intra}})} \qquad \text{(Equation 2)}$$

In this context, the intra-Golgi transport velocity is the highest when the cargo enters the secretory pathway ($t = 0$). However, it is crucial to approach this extrapolation cautiously due to the lack of experimental data at $t \leq 5$ min, when a RUSH reporter's high ER background and low Golgi signal make it challenging to select analyzable Golgi ministacks. It is evident that the dLQ/dt of all our RUSH reporters slows to zero as they transit across the Golgi stack to reach $LQ = y_0$ at the *trans*-Golgi (Figure. 1A-J, right panels), where we propose RUSH reporters exit Golgi ministacks in carriers en route to the plasma membrane(Tie et al., 2018; Tie et al., 2016; Tie et al., 2022). Hence, the intra-Golgi transport velocity of a secretory cargo does not remain constant, contradicting the prediction of the classic cisternal progression model.

Distinct intra-Golgi transport velocities for different cargos at the same cisternae

From Equations 1 and 2, we derive the following relationship (Equation 3):

$$\frac{dLQ}{dt} = \frac{ln2}{t_{intra}}(y_0 - LQ) \qquad \text{(Equation 3)}$$

In our previous work, through side-averaging, we determined that one *LQ* unit corresponds to 274 nm (Tie et al., 2022). Hence, we scaled Equation 3 by 274 nm to derive the instantaneous intra-Golgi transport velocity in nm/min. When plotting the instantaneous intra-Golgi transport velocity (nm/min) against the *LQ* for selected RUSH reporters, as seen in Figure 2A, we observed that different secretory cargos exhibit varied transport velocities even within the same cisternae or at the same *LQ* values. At *LQ* = 0.4, corresponding to the medial-Golgi region, our RUSH reporters' instantaneous intra-Golgi transport velocities are calculated in Table 1 according to Equation 3. For instance, instantaneous intra-Golgi transport velocities of SBP-GFP, SBP-GFP-Tac-TC, SBP-GFP-CD59, SBP-GFP-Tac, and TNFα-SBP-GFP are 6.1, 8.0, 9.2, 14.6, and 20.5 nm/min, respectively (Table 1). These findings highlighted that different secretory cargos possess distinct intra-Golgi transport velocities within the same Golgi cisternae, challenging the prediction made by the classic cisternal progression model.

Golgi residence times vary significantly among different secretory cargos

Once transmembrane secretory cargos transit the Golgi stack, they reach the *trans*-side of the Golgi and are packed into carriers destined for the plasma membrane. The classic cisternal progression model posits that secretory cargos linearly depart the *trans*-Golgi. Contrary to this, cargo exit kinetics have been shown to adhere to a first-order exponential relationship rather than a linear one(Hirschberg et al., 1998; Patterson et al., 2008; Sun et al., 2020). In an attempt to reconcile these observations, Patterson *et al*. introduced the rapid partitioning model, which stands distinct from the classic cisternal progression and stable compartment models(Patterson et al., 2008). This model suggests that cargos rapidly diffuse throughout the Golgi, subsequently segregating into multiple post-translational processing and export domains, where cargos are packed into carriers bound for the plasma membrane. Nonetheless, synchronized traffic waves have been observed through various techniques, including EM(Trucco et al., 2004) and advanced light microscopy methods we developed, such as GLIM and side-averaging(Tie et al., 2016; Tie et al., 2022). These findings suggest

that the rapid partitioning model might not accurately represent the true nature of the intra-Golgi transport.

In both the cisternal progression and stable compartment models, a rapid transit through the Golgi stack, combined with a rate-limiting step at the Golgi exit, could result in the observed exponential Golgi exit kinetics (Luini, 2011). While we could hypothetically apply such a rate-limiting step to both models to rationalize the exponential kinetics of cargo exit, the classic cisternal progression model encounters more significant challenges. Firstly, the first-order exponential Golgi exit implies that clearing a synchronized wave of secretory cargo from the *trans*-cisternae would take an indefinite time, which is inconsistent with the transient nature of the *trans*-cisternae as described by the classic cisternal progression model. Secondly, since cargos are considered passive in the classic cisternal progression model, the exit kinetics, as measured by the Golgi residence times, should be the same across all secretory cargos.

The Golgi residence time is a cargo's duration at the *trans*-Golgi cisternae before exit and is a metric for Golgi retention(Sun et al., 2021; Sun et al., 2020). The first step to determine this metric involves synchronizing a transmembrane protein at the Golgi. For Golgi transmembrane resident proteins like glycosyltransferases and secretory transmembrane proteins with a substantial Golgi localization at the steady state, such as GFP-Tac-TC, synchronization is not required. However, for secretory transmembrane cargos lacking a significant Golgi pool at the steady state, such as TfR-GFP, GFP-Tac, and RUSH reporters like TNFα-SBP-GFP, synchronization is achieved through a 20°C temperature block. Subsequently, live imaging at 37 °C is performed to capture the Golgi fluorescence intensity decay of the protein in the presence of cycloheximide. The Golgi residence time is calculated as the half-time ($t_{1/2}$) by fitting the intensity decay to a first-order exponential function.

Our extensive measurement demonstrated that Golgi residence times of secretory cargos display a wide range of values (Table 2). For example, TNFα-SBP-GFP has a Golgi residence time of 6.0 ± 0.4 min (n = 73), one of the shortest, while SBP-GFP-CD59 has a Golgi residence time of 16 ± 2 min (n = 29) (Supplementary Fig. 2A). Hence, our data suggest that different

secretory cargos reside at the *trans*-Golgi cisternae for varying durations, contradicting predictions from the classic cisternal progression model.

Cargos exhibiting prolonged Golgi residence times suggest the *trans*-Golgi interior might be a stable domain

The classic cisternal progression model could be modified to explain the diverse transport kinetics. For example, accelerated anterograde or retrograde transport might be introduced on top of the basal cisternal progression to account for the wide range of intra-Golgi transport velocities and Golgi residence times we observed (Fig. 2B). Accelerated anterograde transport mechanisms might include continuity-based direct diffusion across cisternae via heterologous cisternal connections(Beznoussenko et al., 2014; Marsh et al., 2004; Trucco et al., 2004). Hence, secretory cargo with such a mechanism would have a faster intra-Golgi transport velocity. This mechanism might explain the rapid and diverse intra-Golgi transport velocity of secretory cargos such as VSVG, insulin, albumin, and alpha1-antitrypsin(Beznoussenko et al., 2014; Marsh et al., 2004; Trucco et al., 2004). Similarly, active recruitment to exocytic carriers budding at the *trans*-Golgi possibly might shorten the Golgi residence time. On the other hand, COPI-coated carriers might facilitate retrograde intra-Golgi transport to counter the cisternal progression, accounting for the slow intra-Golgi transport velocity and prolonged Golgi residence time of cargos. Indeed, COPI has been known to maintain certain glycosyltransferases' Golgi retention by direct or indirect interactions (Ali et al., 2012; Eckert et al., 2014; Liu et al., 2018; Pereira et al., 2014; Rizzo et al., 2021; Schmitz et al., 2008; Tu et al., 2008). However, such a retrograde mechanism requires the interaction between secretory cargo and the COPI coat.

Earlier, we identified truncation mutants of two typical secretory cargos, GFP-Tac and GFP-CD8a, which reside in the Golgi nearly as stably as Golgi glycosyltransferases(Sun et al., 2020). These are type I transmembrane proteins comprising from their N- to C-termini a signal peptide, GFP, luminal domain, transmembrane domain (TMD), and cytosolic tail (Fig. 3A). Previously, we and others demonstrated that fully glycosylated luminal domain can function

as a Golgi exit signal (Gut et al., 1998; Sun et al., 2020). Their Golgi residence time was documented at 16 ± 2 min (*n* = 45) and 7.8 ± 0.7 min (*n* = 26), respectively (Table 2). However, after truncating the luminal domain, the Golgi residence time for the resultant chimeras, GFP-Tac-TC and GFP-CD8a-TC, extended significantly to 3.4 ± 0.3 h (*n* = 22) and 66 ± 7 min (*n* = 19) (Table 2)(Supplementary Fig. 2B), respectively. Consequentially, their long Golgi residence times ensure a significant steady-state Golgi pool.

The following evidence suggests that GFP-Tac-TC behaves like a bona fide Golgi resident transmembrane protein. Firstly, its Golgi residence time, 3.4 h, is comparable to that of a typical Golgi glycosyltransferase, such as ST6GAL1 (5.3 ± 0.6 h, *n* = 21)(Sun et al., 2021). Second, GFP-Tac-TC follows GalT-mCherry to localize to the ER under the BFA treatment reversibly (Sun et al., 2020). Third, GFP-Tac-TC's *LQ*, 0.94 ± 0.02 (*n* = 118), combined with its cisternal interior localization(Sun et al., 2020), indicates that it primarily resides within the interior of the *trans*-cisternae, similar to many Golgi glycosyltransferases(Tie et al., 2018).

According to the modified cisternal progression model above, GFP-Tac-Tc could have an active retrieval mechanism mediated by an unidentified signal in its cytosolic tail or TMD to counter the cisternal progression. Considering that GFP-Tac-TC's *LQ*, 0.94 ± 0.02 (*n* = 118), is close to its Golgi exit site, y_0 (0.94 – 1.05) (Table 1; Fig. 1 E and Supplementary Fig. 1C), measured by its RUSH version, there are two possible retrieval pathways, acting at either post-Golgi or intra-Golgi stages. To test if GFP-Tac-Tc possesses a Golgi retrieval pathway after its Golgi exit, we incubated HeLa cells transiently expressing MGAT1-GFP (negative control)(Sun et al., 2021), MGAT2-GFP (positive control)(Sun et al., 2021), GFP-Tac, or GFP-Tac-TC with a recombinant mCherry-fused anti-GFP nanobody (VHH-anti-GFP-mCherry) continuously for 8 h (Fig. 3B). We found that VHH-anti-GFP-mCherry localized to the Golgi in a significant fraction of MAGT2-GFP-expressing cells (41%, *n* = 81) but not in MGAT1-GFP cells (0%, *n* = 102). This result is consistent with our previous report that MGAT2, but not MAGT1, has a Golgi retrieval mechanism(Sun et al., 2021), although its molecular mechanism is still unknown. In contrast, VHH-anti-GFP-mCherry did not localize to the Golgi in cells

expressing other constructs, including GFP-Tac-TC, suggesting that GFP-Tac-TC might not possess a post-Golgi retrieval mechanism targeting the Golgi. Next, we reason that given GFP-Tac's short Golgi residence time (16 ± 2 min, n = 45), its cytosolic tail and TMD might not facilitate any active intra-Golgi retrograde transport mechanism, such as COPI coat binding, to recycle GFP-Tac-TC from Golgi exiting. Since GFP-Tac and GFP-Tac-TC share identical TMD and cytosolic tail sequences, if such a retrograde mechanism existed, GFP-Tac would have a similar Golgi residence time to GFP-Tac-TC. The same observation and reasoning also apply to GFP-CD8a-TC (Fig. 3B). Therefore, we argue that GFP-Tac-TC and GFP-CD8a-TC might not have retrieval signal to facilitate their Golgi residence, although proving a protein does not possess a transport signal is challenging. Since the cisternal interior is continuous with the cisternal rim both in membrane and lumen, our findings suggest that the cisternal interior at the *trans*-Golgi might be a stable domain. Our findings suggest that retention within the *trans*-side stable domain, rather than continuous retrieval to counter the cisternal progression (treadmilling), could be the primary mechanism for the long Golgi residence times of GFP-Tac-TC and GFP-CD8a-TC.

We have previously demonstrated in fluorescence microscopy that during their intra-Golgi transition, small cargos, such as CD59, E-cadherin, and VSVG, localize to the cisternal interior, coinciding with Golgi glycosyltransferases, while large cargos, such as FM4 aggregates and collagenX, position themselves at the cisternal rim, where trafficking machinery components localize(Tie et al., 2018). The rim partitioning of large secretory cargos is consistent with previous EM studies of procollagen I(Bonfanti et al., 1998), FM4 aggregates(Lavieu et al., 2013), and algal protein aggregates(Engel et al., 2015). Therefore, these findings might support a modified version of the stable compartment model — the rim progression model (Lavieu et al., 2013; Pfeffer, 2010; Volchuk et al., 2000). In this model, each Golgi cisterna seems to have a stable interior domain and a dynamic rim domain; the rim domain of Golgi cisternae undergoes constant en bloc fission and fusion for intra-Golgi cargo transport. The rim progression model can readily explain the diverse intra-Golgi transport velocities, the

exponential Golgi exit, and the wide range of Golgi residence times of secretory cargos. It also helps explain the retention of Golgi glycosyltransferases at the cisternal interior since many do not recycle via COPI-coated vesicles(Liu et al., 2018) or possess a post-Golgi retrieval pathway(Sun et al., 2021). The Golgi glycosyltransferase at the cisternal interior might assemble a dense protein matrix based on fluorescence (Tie et al., 2018) and EM data(Engel et al., 2015). It is tempting to speculate that the glycosyltransferase matrix could functionally mirror a gel-filtration chromatography matrix with a defined porosity. Hence, large secretory cargos, such as FM4 aggregates and collagenX, are excluded from the interior, where the glycosyltransferase matrix localizes, while small secretory cargos can enter and become kinetically trapped there.

The Golgi maintains its stacked organization after 30 min BFA treatment

COPI functions in the retrograde direction at the ER-Golgi interface and within the Golgi (Glick and Luini, 2011; Popoff et al., 2011; Rabouille and Klumperman, 2005). According to the classic cisternal progression model, COPI-mediated retrograde intra-Golgi transport recycles resident transmembrane proteins, such as glycosyltransferases and transport machinery components. This model predicts that upon the compromisation of COPI, intra-Golgi recycling would stop, and the Golgi stack would continuously lose its materials and eventually disappear, depending on the cisternal progression rate. In addition to its retrograde role, COPI has also been documented to function in the anterograde ER-to-Golgi transport(Monetta et al., 2007; Weigel et al., 2021).

To test the role of COPI in the Golgi organization, we employed BFA, a small-molecule fungal metabolite that rapidly dissociates COPI and clathrin from the Golgi, inhibits the ER-to-Golgi trafficking, and causes the fusion of the Golgi with the ER in 10 - 20 min(Klausner et al., 1992). It does so by rapidly inactivating class I ARFs, which recruit COPI and clathrin coats to the Golgi membrane(Donaldson et al., 1992; Helms and Rothman, 1992). In contrast to the native Golgi, nocodazole-induced Golgi ministacks have been documented to be more resistant to BFA, and, hence, the disappearance of Golgi occurs at a much later time (> 30 min)(Lippincott-

Schwartz et al., 1990). However, it is unclear if the nocodazole-induced Golgi maintains a similar stacked organization under the BFA treatment.

Given this, we studied the *LQ*s of several Golgi markers under 30 – 60 min BFA treatment (Fig. 4). The fast dissociation of Arf1-GFP from Golgi ministacks confirmed the effectiveness of BFA (Supplementary Fig. 3). We also observed that extended BFA treatment considerably reduced intact Golgi ministacks. We measured the *LQ*s of five transmembrane Golgi markers, GFP-golgin-84, GS15, ST6GAL1-GFP, TGN46, CD8a-furin, and CD8a-CI-M6PR (Fig. 4). GS15's *LQ* was monitored for 60 min, with the rest for 30 min. We observed that *LQ*s of ST6GAL1 and GS15 did not change significantly, while the *LQ* of golgin-84 increased from 0.2 to 0.4. Remarkably, *LQ*s of all three TGN markers decreased and approached that of the *trans*-Golgi, suggesting a collapse of the TGN, possibly due to the dissociation of clathrin and its adaptor proteins. In summary, despite dramatic changes in the TGN, *LQ*s of tested Golgi stack markers still follow a similar arrangement to those of pre-BFA treatment. Therefore, our data demonstrate that the Golgi maintains its stacked organization for at least 30 – 60 min, even in the absence of COPI-mediated intra-Golgi retrograde transport. Our findings suggest that the Golgi might not be a dynamic equilibrium between the cisternal progression and retrograde trafficking and argue for a by-default stable nature of the Golgi stack. It is worth noting that the cellular effect of BFA is complex and pleiotropic. For example, in addition to Arfs, it can inhibit lipid metabolic enzymes(De Matteis et al., 1994). So, the disassociation of COPI might not be the sole factor responsible for our observations.

Summary

We introduced new quantitative data on the intra-Golgi transport dynamics. However, our study has limitations. First, our approach relied on the overexpression of fluorescence protein-tagged cargos. The synchronized release of a large amount of cargo could significantly saturate and skew the intra-Golgi transport. Second, we utilized nocodazole-induced ministacks instead of the native Golgi to analyze the intra-Golgi transport, which could raise

concerns about the impact of depolymerizing microtubules on the intra-Golgi transport and Golgi organization.

Our findings suggest that the Golgi cisternal interior might be a stable domain, therefore supporting a modified version of the stable compartment model, the rim progression model. However, we do not think our data alone can resolve the two models, which have been the subject of debate for several decades. Further refinement of the classic cisternal progression model might also account for our data. We anticipate further development using our approach will provide more systematic data to test and refine future intra-Golgi transport models. Moreover, we hope that our study will stimulate further research into this longstanding and intriguing question.

Materials and methods

DNA plasmids, antibodies, and small molecules

To clone RUSH reporter, SBP-GFP, two PCRs were performed using li-Strep_ss-SBP-EGFP-Ecadherin (a gift plasmid from F. Perez) (Boncompain et al., 2012) and pEGFP-C1 (Clontech) as templates and the following primer pairs (GAT GCA CCC GGG AGG CGC GCC ATG and CTC CTC GCC CTT GCT CAC ACC TGC AGG TGG TTC ACG) and (CGT GAA CCA CCT GCA GGT GTG AGC AAG GGC GAG GAG and GAT GCA TCT AGA TTA CTT GTA CAG CTC GTC CAT), respectively. The mixture of the two purified PCR fragments was used as the template for the third round of PCR amplification using the first and the fourth primer listed above. The resulting PCR fragment was digested by XmaI and XbaI and ligated to XmaI and XbaI digested li-Strep_ss-SBP-EGFP-Ecadherin DNA plasmid. To clone GFP-CD8a-TC, the coding sequence of the TMD and cytosolic tail of CD8a was amplified by PCR using GFP-CD8a(Sun et al., 2020) as a template and the following primers, CAG TGC CTC GAG GAC TTC GCC TGT GAT ATC TA and GAC CGT GAA TTC TTA GAC GTA TCT CGC CGA AAG GCT G. The resulting PCR fragment was digested by EcoRI and XhoI and ligated to EcoRI and XhoI digested GFP-CD8a DNA plasmid.

ST6GAL1-GFP (ST-GFP) (Sun et al., 2020), CD8a-furin(Mahajan et al., 2013), CD8a-CI-M6PR(Mahajan et al., 2013) were previously described. RUSH TfR-SBP-GFP was a gift plasmid from J. Bonifacino (Chen et al., 2017). GFP-golgin-84 (Diao et al., 2003) was a gift plasmid from M. Lowe. Arf1-GFP(Wessels et al., 2006) was a gift plasmid from F. van Kuppeveld.

Mouse monoclonal antibody anti-CD8a (OKT8) was from the hybridoma culture supernatant. Mouse monoclonal antibodies against GM130 (#610822) and GS15 (#610960) were purchased from BD Bioscience. Rabbit polyclonal antibody against TGN46 was from Abcam (#ab50595). Alexa Fluor 488, 594, and 647-conjugated goat anti-mouse or anti-rabbit secondary antibodies were purchased from Thermo Fisher Scientific.

Small molecules

Nocodazole (#487928; working concentration: 33 μM), brefeldin A (working concentration: 10 μg/ml), and cycloheximide (working concentration: 10 μg/ml) were purchased from Merck, Epicenter Technologies, and Sigma Aldrich, respectively.

Cell culture and transfection

HeLa cells were maintained in Dulbecco's Modified Eagle's Medium (DMEM) supplemented with 10% fetal bovine serum (FBS) to make it complete DMEM. For cell transfection, Lipofectamine 2000 (Thermal Fisher Scientific) was used per the manufacturer's instructions. For BFA treatment, cells were treated with complete DMEM containing 1 μM BFA for the specified duration. For nocodazole treatment, cells were treated with complete DMEM containing 33 μM nocodazole for 3 hours to induce the formation of Golgi ministacks.

Immunofluorescence

Cells for immunofluorescence were grown on No. 1.5 Φ12 mm glass coverslips. They were fixed using 4% paraformaldehyde in phosphate-buffered saline (PBS). Following a PBS wash to remove residual paraformaldehyde, any remaining paraformaldehyde within the cells was neutralized with 100 mM NH_4Cl. The cells were then processed for immunofluorescence labeling by first incubating with mouse or rabbit primary antibodies, followed by Alexa Fluor 488, 594, and/or 647 conjugated goat anti-mouse or anti-rabbit secondary antibodies. Both primary and secondary antibodies were diluted in PBS containing 5% fetal bovine serum, 2% bovine serum albumin, and 0.1% saponin (Sigma-Aldrich). The labeled cells were mounted in the Mowiol mounting medium, composed of 12% Mowiol 4-88 (EMD Millipore), 30% glycerol, and 100 mM Tris pH 8.5. After the mounting medium had dried, the coverslips were sealed with nail polish and stored at - 20°C.

Acquiring *LQ*s

To analyze *LQ*s of intra-Golgi transport RUSH reporters, HeLa cells transiently co-expressing individual GFP-tagged RUSH reporter and GalT-mCherry were cultured in complete DMEM supplemented with16 nM His-tagged streptavidin (in-house purified using Addgene #20860, a gift plasmid from A. Ting)(Howarth et al., 2006). Following a 3 h nocodazole treatment, cells were chased with 40 μM biotin, 10 μg/ml cycloheximide, and 33 μM nocodazole for various durations before fixation.

In another set of experiments to study *LQ*s of Golgi markers under the BFA treatment, nocodazole-treated HeLa cells transiently expressing GalT-mCherry were further incubated with 1 μM BFA and 33 μM nocodazole for various durations before fixation. For these experiments, the Golgi markers were either co-expressed with GalT-mCherry as a GFP-tagged construct or detected as an endogenous protein by immunostaining.

The methodology for acquiring *LQ*s through GLIM has been described in our previous studies(Tie et al., 2017; Tie et al., 2016). Briefly, cells were further immuno-labeled to visualize endogenous GM130. Ministacks exhibiting fluorescence signals of GM130, transfected GalT-mCherry, and the testing protein were imaged using a wide-field microscope. Ministacks were manually selected for analysis, and fluorescence centers for GM130, GalT-mCherry, and the testing protein were acquired using Fiji (https://imagej.net/software/fiji/). After chromatic aberration correction, coordinates of fluorescence centers were used to calculate *LQ*s, defined as the ratio of axial distances from GM130 to the testing protein and from GM130 to GalT-mCherry. Intra-Golgi transport kinetic *LQ* data were fitted to the first-order exponential function using OriginPro 2020.

Acquisition of Golgi residence times

The methodology follows protocols previously described(Sun et al., 2021; Sun et al., 2020). Nocodazole was not used in these experiments. Briefly, HeLa cells on a Φ 35mm glass-bottom Petri dish were transiently transfected to co-express a GFP-tagged reporter and GalT-mCherry. For RUSH reporters, cells were treated with 40 μM biotin at 20 °C for 2 hours to

accumulate the reporter at the Golgi. Live imaging was performed in a CO_2-independent medium (Thermo Fisher Scientific) with 10% FBS, 4 mM glutamine, and 10 μg/ml cycloheximide, using a wide-field microscope until the cellular GFP fluorescence at the Golgi nearly vanished. The resulting time-lapse images were segmented based on GalT-mCherry using Fiji. Total GFP fluorescence within the Golgi was quantified and fitted to the first-order exponential function $y = y0 + A1\exp(-x/t1)$ in OriginPro 2020. Golgi residence time, $t_{1/2}$, was calculated as $0.693*t1$. We only included time-lapse data with adj. $R^2 \geq 0.80$ and acquisition length $\geq 1.33*t_{1/2}$.

VHH-anti-GFP-mCherry internalization assay

6 × His-tagged VHH-anti-GFP-mCherry was purified as previously described(Sun et al., 2021; Sun et al., 2020). In the interanlization assay, HeLa cells transiently expressing GFP-tagged reporters were continuously incubated with 5 μg/ml VHH-anti-GFP-mCherry at 37 °C for 8 h. After washing, cells were fixed and imaged.

Wide-field microscopy

*LQ*s and Golgi residence times were measured using a wide-field microscope based on Olympus IX83. The microscope featured a 100× oil objective lens (NA 1.40), a motorized stage for sample positioning, and automated filter cubes to accommodate different fluorescence channels. Dichroic mirrors and filters were optimized for GFP/Alexa fluor 488, mCherry/Alexa Fluor 594, and Alexa Fluor 647. Imaging was captured with an sCMOS (scientific complementary metal oxide semiconductor) camera (Neo) by Andor. A 200W metal halide light source (Lumen Pro 200) by Prior Scientific provided illumination. Operational control and data collection were facilitated through Metamorph software by Molecular Devices.

Airyscan microscopy

The Airyscan microscopy was performed using a Zeiss LSM710 confocal microscope, equipped with alpha Plan-Apochromat 100× NA 1.46 objective and the Airyscan module (Carl

Zeiss). The system operation was controlled by Zen software (Carl Zeiss). Two lines of laser lights were used, 488 and 640 nm. The emission band was selected to optimize the capture of the emission light while minimizing channel crosstalk.

Declaration of interests

The authors declare no competing interests.

Acknowledgment

We want to thank J. Bonifacino (National Institute of Health, USA), F. van Kuppeveld (Utrecht University), M. Lowe (University of Manchester, UK), F. Perez (Institute of Curie, France), and A. Ting (Stanford University, USA) for sharing DNA plasmids. This project is supported by the Ministry of Education, Singapore, under its Tier 2 MOE-T2EP30221-0001 and Tier 1 RG 25/22.

Table 1

Intra-Golgi transport kinetics of secretory RUSH reporters in Golgi ministacks. See the legend of Figure 1 for details. #1-3 indicate independent replicates. Except for TNFα-SBP-GFP, which uses Ii-Streptavidin as the ER hook, all RUSH reporters employ signal sequence fused streptavidin-KDEL as their ER hook. Superscripts 1 and 2 indicate data were re-analyzed from previous publications (Tie et al., 2016) and (Sun et al., 2020). WT, wild type. t_{intra} (intra-Golgi transport time), y_0, and adj. R^2 were calculated by fitting measured *LQ* vs. time kinetics data to Equation 1. d*LQ*/d*t* (at *LQ* = 0.4) was calculated by Equation 3, and converted to nm/min by multiplying 274 nm per *LQ* unit. For furin cytosolic tail RUSH reporters, YA is YKGL, a tyrosine-based motif, to AKGL mutation, while AC is SDSEEDE, an acidic cluster sequence, to ADAAAAA mutation(Tie et al., 2016). YA + AC indicates mutations in both sites (Tie et al., 2016).

RUSH reporter	t_{intra} (min)	y_0	Adj. R^2	d*LQ*/d*t* (at *LQ* = 0.4)	d*LQ*/dt (at *LQ* = 0.4) (nm/min)
TNFα-SBP-GFP[1]	6.4	1.09	0.94	0.075	20.5
SBP-GFP-CD59[1]	13.0	1.03	0.97	0.034	9.2
SBP-GFP	10.6	0.74	0.98	0.022	6.1
SBP-GFP-Tac #1[2]	6.0	0.86	0.98	0.053	14.6
SBP-GFP-Tac #2	8.2	0.91	0.98	0.043	11.8
SBP-GFP-Tac-TC #1[2]	15.5	1.05	0.97	0.029	8.0
SBP-GFP-Tac-TC #2	19.1	1.16	0.94	0.028	7.6
TfR-SBP-GFP	7.0	1.16	0.99	0.075	20.6
SBP-GFP-E-cadherin #1[1]	7.6	0.98	0.99	0.053	14.5
SBP-GFP-E-cadherin #2[1]	8.7	1.15	0.96	0.060	16.5
SBP-GFP-E-cadherin #3[1]	6.5	1.11	0.98	0.075	20.6
SBP-GFP-CD8a-furin-WT #1[1]	23.6	1.63	0.96	0.036	9.9
SBP-GFP-CD8a-furin-WT #2[1]	18.7	1.58	0.97	0.044	12.0
SBP-GFP-CD8a-furin-WT #3[1]	13.1	1.55	0.97	0.061	16.7
SBP-GFP-CD8a-furin-YA #1[1]	5.9	1.49	0.98	0.128	35.0
SBP-GFP-CD8a-furin-YA #2[1]	11.1	1.51	0.93	0.069	19.0
SBP-GFP-CD8a-furin-YA #3[1]	16.3	1.48	0.95	0.046	12.6
SBP-GFP-CD8a-furin-AC #1[1]	17.9	1.73	0.99	0.052	14.1
SBP-GFP-CD8a-furin-AC #2[1]	26.9	1.50	1.00	0.028	7.8

SBP-GFP-CD8a-furin-AC #3[1]	23.2	1.58	0.96	0.035	9.7
SBP-GFP-CD8a-furin-Y+AC #1[1]	4.9	0.83	0.99	0.061	16.7
SBP-GFP-CD8a-furin-Y+AC #2[1]	7.1	1.00	0.99	0.059	16.0
SBP-GFP-CD8a-furin-Y+AC #3[1]	7.7	1.04	0.92	0.058	15.8

Table 2

Golgi residence times of transmembrane secretory cargos and Golgi glycosyltransferases in native Golgi (without nocodazole). Superscripts 1 and 2 indicate data were from previous publications (Sun et al., 2020) and (Sun et al., 2021), respectively. The RUSH reporter, TNFα-SBP-GFP, employs signal sequence fused streptavidin-KDEL as the ER hook. *n*, the number of quantified cells; SEM, standard error of the mean.

Transmembrane protein	Golgi residence time ($t_{1/2}$)	*n*	SEM
TNFα-SBP-GFP[1]	6.0 min	73	0.4 min
GFP-CD8a[1]	7.8 min	26	0.7 min
TfR-GFP[1]	10 min	12	1 min
GFP-Tac[1]	16 min	45	2 min
SBP-GFP-CD59	16 min	29	2 min
GFP-Tac (5A)[1]	47 min	57	3 min
GFP-CD8a-TC	66 min	19	7 min
GFP-Tac-TC[1]	3.4 h	22	0.3 h
MGAT2-GFP[2]	4.9 h	26	0.5 h
ST6GAL1-GFP[1]	5.3 h	21	0.6 h

References

Ali, M.F., V.B. Chachadi, A. Petrosyan, and P.W. Cheng. 2012. Golgi phosphoprotein 3 determines cell binding properties under dynamic flow by controlling Golgi localization of core 2 N-acetylglucosaminyltransferase 1. *J Biol Chem*. 287:39564-39577.

Beznoussenko, G.V., S. Parashuraman, R. Rizzo, R. Polishchuk, O. Martella, D. Di Giandomenico, A. Fusella, A. Spaar, M. Sallese, M.G. Capestrano, M. Pavelka, M.R. Vos, Y.G. Rikers, V. Helms, A.A. Mironov, and A. Luini. 2014. Transport of soluble proteins through the Golgi occurs by diffusion via continuities across cisternae. *Elife*. 3.

Boncompain, G., S. Divoux, N. Gareil, H. de Forges, A. Lescure, L. Latreche, V. Mercanti, F. Jollivet, G. Raposo, and F. Perez. 2012. Synchronization of secretory protein traffic in populations of cells. *Nat Methods*. 9:493-498.

Bonfanti, L., A.A. Mironov, Jr., J.A. Martinez-Menarguez, O. Martella, A. Fusella, M. Baldassarre, R. Buccione, H.J. Geuze, A.A. Mironov, and A. Luini. 1998. Procollagen traverses the Golgi stack without leaving the lumen of cisternae: evidence for cisternal maturation. *Cell*. 95:993-1003.

Chen, Y., D.C. Gershlick, S.Y. Park, and J.S. Bonifacino. 2017. Segregation in the Golgi complex precedes export of endolysosomal proteins in distinct transport carriers. *J Cell Biol*. 216:4141-4151.

Cole, N.B., N. Sciaky, A. Marotta, J. Song, and J. Lippincott-Schwartz. 1996. Golgi dispersal during microtubule disruption: regeneration of Golgi stacks at peripheral endoplasmic reticulum exit sites. *Mol Biol Cell*. 7:631-650.

De Matteis, M.A., M. Di Girolamo, A. Colanzi, M. Pallas, G. Di Tullio, L.J. McDonald, J. Moss, G. Santini, S. Bannykh, D. Corda, and et al. 1994. Stimulation of endogenous ADP-ribosylation by brefeldin A. *Proc Natl Acad Sci U S A*. 91:1114-1118.

De Matteis, M.A., and A. Luini. 2008. Exiting the Golgi complex. *Nat Rev Mol Cell Biol*. 9:273-284.

Diao, A., D. Rahman, D.J. Pappin, J. Lucocq, and M. Lowe. 2003. The coiled-coil membrane protein golgin-84 is a novel rab effector required for Golgi ribbon formation. *J Cell Biol*. 160:201-212.

Donaldson, J.G., D. Finazzi, and R.D. Klausner. 1992. Brefeldin A inhibits Golgi membrane-catalysed exchange of guanine nucleotide onto ARF protein. *Nature*. 360:350-352.

Eckert, E.S., I. Reckmann, A. Hellwig, S. Rohling, A. El-Battari, F.T. Wieland, and V. Popoff. 2014. Golgi phosphoprotein 3 triggers signal-mediated incorporation of glycosyltransferases into coatomer-coated (COPI) vesicles. *J Biol Chem*. 289:31319-31329.

Emr, S., B.S. Glick, A.D. Linstedt, J. Lippincott-Schwartz, A. Luini, V. Malhotra, B.J. Marsh, A. Nakano, S.R. Pfeffer, C. Rabouille, J.E. Rothman, G. Warren, and F.T. Wieland. 2009. Journeys through the Golgi--taking stock in a new era. *J Cell Biol*. 187:449-453.

Engel, B.D., M. Schaffer, S. Albert, S. Asano, J.M. Plitzko, and W. Baumeister. 2015. In situ structural analysis of Golgi intracisternal protein arrays. *Proc Natl Acad Sci U S A*. 112:11264-11269.

Fourriere, L., S. Divoux, M. Roceri, F. Perez, and G. Boncompain. 2016. Microtubule-independent secretion requires functional maturation of Golgi elements. *J Cell Sci*. 129:3238-3250.

Glick, B.S., and A. Luini. 2011. Models for Golgi traffic: a critical assessment. *Cold Spring Harb Perspect Biol*. 3:a005215.

Gut, A., F. Kappeler, N. Hyka, M.S. Balda, H.P. Hauri, and K. Matter. 1998. Carbohydrate-mediated Golgi to cell surface transport and apical targeting of membrane proteins. *EMBO J*. 17:1919-1929.

Helms, J.B., and J.E. Rothman. 1992. Inhibition by brefeldin A of a Golgi membrane enzyme that catalyses exchange of guanine nucleotide bound to ARF. *Nature*. 360:352-354.

Hirschberg, K., C.M. Miller, J. Ellenberg, J.F. Presley, E.D. Siggia, R.D. Phair, and J. Lippincott-Schwartz. 1998. Kinetic analysis of secretory protein traffic and characterization of golgi to plasma membrane transport intermediates in living cells. *J Cell Biol*. 143:1485-1503.

541 Howarth, M., D.J. Chinnapen, K. Gerrow, P.C. Dorrestein, M.R. Grandy, N.L. Kelleher, A. El-Husseini,
542 and A.Y. Ting. 2006. A monovalent streptavidin with a single femtomolar biotin binding site.
543 *Nat Methods*. 3:267-273.
544 Klausner, R.D., J.G. Donaldson, and J. Lippincott-Schwartz. 1992. Brefeldin A: insights into the control
545 of membrane traffic and organelle structure. *J Cell Biol*. 116:1071-1080.
546 Klumperman, J. 2011. Architecture of the mammalian Golgi. *Cold Spring Harb Perspect Biol*. 3.
547 Kurokawa, K., H. Osakada, T. Kojidani, M. Waga, Y. Suda, H. Asakawa, T. Haraguchi, and A. Nakano.
548 2019. Visualization of secretory cargo transport within the Golgi apparatus. *J Cell Biol*.
549 218:1602-1618.
550 Lavieu, G., H. Zheng, and J.E. Rothman. 2013. Stapled Golgi cisternae remain in place as cargo passes
551 through the stack. *Elife*. 2:e00558.
552 Lippincott-Schwartz, J., J.G. Donaldson, A. Schweizer, E.G. Berger, H.P. Hauri, L.C. Yuan, and R.D.
553 Klausner. 1990. Microtubule-dependent retrograde transport of proteins into the ER in the
554 presence of brefeldin A suggests an ER recycling pathway. *Cell*. 60:821-836.
555 Liu, L., B. Doray, and S. Kornfeld. 2018. Recycling of Golgi glycosyltransferases requires direct binding
556 to coatomer. *Proc Natl Acad Sci U S A*. 115:8984-8989.
557 Losev, E., C.A. Reinke, J. Jellen, D.E. Strongin, B.J. Bevis, and B.S. Glick. 2006. Golgi maturation
558 visualized in living yeast. *Nature*. 441:1002-1006.
559 Luini, A. 2011. A brief history of the cisternal progression-maturation model. *Cell Logist*. 1:6-11.
560 Mahajan, D., B.K. Boh, Y. Zhou, L. Chen, T.C. Cornvik, W. Hong, and L. Lu. 2013. Mammalian
561 Mon2/Ysl2 regulates endosome-to-Golgi trafficking but possesses no guanine nucleotide
562 exchange activity toward Arl1 GTPase. *Sci Rep*. 3:3362.
563 Marsh, B.J., N. Volkmann, J.R. McIntosh, and K.E. Howell. 2004. Direct continuities between
564 cisternae at different levels of the Golgi complex in glucose-stimulated mouse islet beta
565 cells. *Proc Natl Acad Sci U S A*. 101:5565-5570.
566 Matsuura-Tokita, K., M. Takeuchi, A. Ichihara, K. Mikuriya, and A. Nakano. 2006. Live imaging of
567 yeast Golgi cisternal maturation. *Nature*. 441:1007-1010.
568 Mironov, A.A., G.V. Beznoussenko, P. Nicoziani, O. Martella, A. Trucco, H.S. Kweon, D. Di
569 Giandomenico, R.S. Polishchuk, A. Fusella, P. Lupetti, E.G. Berger, W.J. Geerts, A.J. Koster,
570 K.N. Burger, and A. Luini. 2001. Small cargo proteins and large aggregates can traverse the
571 Golgi by a common mechanism without leaving the lumen of cisternae. *J Cell Biol*. 155:1225-
572 1238.
573 Monetta, P., I. Slavin, N. Romero, and C. Alvarez. 2007. Rab1b interacts with GBF1 and modulates
574 both ARF1 dynamics and COPI association. *Mol Biol Cell*. 18:2400-2410.
575 Patterson, G.H., K. Hirschberg, R.S. Polishchuk, D. Gerlich, R.D. Phair, and J. Lippincott-Schwartz.
576 2008. Transport through the Golgi apparatus by rapid partitioning within a two-phase
577 membrane system. *Cell*. 133:1055-1067.
578 Pereira, N.A., H.X. Pu, H. Goh, and Z. Song. 2014. Golgi phosphoprotein 3 mediates the Golgi
579 localization and function of protein O-linked mannose beta-1,2-N-
580 acetylglucosaminyltransferase 1. *J Biol Chem*. 289:14762-14770.
581 Pfeffer, S.R. 2010. How the Golgi works: a cisternal progenitor model. *Proc Natl Acad Sci U S A*.
582 107:19614-19618.
583 Popoff, V., F. Adolf, B. Brugger, and F. Wieland. 2011. COPI budding within the Golgi stack. *Cold*
584 *Spring Harb Perspect Biol*. 3:a005231.
585 Rabouille, C., and J. Klumperman. 2005. Opinion: The maturing role of COPI vesicles in intra-Golgi
586 transport. *Nat Rev Mol Cell Biol*. 6:812-817.
587 Rizzo, R., D. Russo, K. Kurokawa, P. Sahu, B. Lombardi, D. Supino, M.A. Zhukovsky, A. Vocat, P.
588 Pothukuchi, V. Kunnathully, L. Capolupo, G. Boncompain, C. Vitagliano, F. Zito Marino, G.
589 Aquino, D. Montariello, P. Henklein, L. Mandrich, G. Botti, H. Clausen, U. Mandel, T. Yamaji,
590 K. Hanada, A. Budillon, F. Perez, S. Parashuraman, Y.A. Hannun, A. Nakano, D. Corda, G.

591 D'Angelo, and A. Luini. 2021. Golgi maturation-dependent glycoenzyme recycling controls
592 glycosphingolipid biosynthesis and cell growth via GOLPH3. *EMBO J*. 40:e107238.
593 Rogalski, A.A., J.E. Bergmann, and S.J. Singer. 1984. Effect of microtubule assembly status on the
594 intracellular processing and surface expression of an integral protein of the plasma
595 membrane. *J Cell Biol*. 99:1101-1109.
596 Schmitz, K.R., J. Liu, S. Li, T.G. Setty, C.S. Wood, C.G. Burd, and K.M. Ferguson. 2008. Golgi
597 localization of glycosyltransferases requires a Vps74p oligomer. *Dev Cell*. 14:523-534.
598 Sun, X., D. Mahajan, B. Chen, Z. Song, and L. Lu. 2021. A quantitative study of the Golgi retention of
599 glycosyltransferases. *J Cell Sci*. 134.
600 Sun, X., H.C. Tie, B. Chen, and L. Lu. 2020. Glycans function as a Golgi export signal to promote the
601 constitutive exocytic trafficking. *J Biol Chem*. 295:14750-14762.
602 Tie, H.C., B. Chen, X. Sun, L. Cheng, and L. Lu. 2017. Quantitative Localization of a Golgi Protein by
603 Imaging Its Center of Fluorescence Mass. *J Vis Exp*.
604 Tie, H.C., A. Ludwig, S. Sandin, and L. Lu. 2018. The spatial separation of processing and transport
605 functions to the interior and periphery of the Golgi stack. *Elife*. 7.
606 Tie, H.C., D. Mahajan, B. Chen, L. Cheng, A.M. VanDongen, and L. Lu. 2016. A novel imaging method
607 for quantitative Golgi localization reveals differential intra-Golgi trafficking of secretory
608 cargoes. *Mol Biol Cell*. 27:848-861.
609 Tie, H.C., D. Mahajan, and L. Lu. 2022. Visualizing intra-Golgi localization and transport by side-
610 averaging Golgi ministacks. *J Cell Biol*. 221.
611 Trucco, A., R.S. Polishchuk, O. Martella, A. Di Pentima, A. Fusella, D. Di Giandomenico, E. San Pietro,
612 G.V. Beznoussenko, E.V. Polishchuk, M. Baldassarre, R. Buccione, W.J. Geerts, A.J. Koster,
613 K.N. Burger, A.A. Mironov, and A. Luini. 2004. Secretory traffic triggers the formation of
614 tubular continuities across Golgi sub-compartments. *Nat Cell Biol*. 6:1071-1081.
615 Tu, L., W.C. Tai, L. Chen, and D.K. Banfield. 2008. Signal-mediated dynamic retention of
616 glycosyltransferases in the Golgi. *Science*. 321:404-407.
617 Van De Moortele, S., R. Picart, A. Tixier-Vidal, and C. Tougard. 1993. Nocodazole and taxol affect
618 subcellular compartments but not secretory activity of GH3B6 prolactin cells. *Eur J Cell Biol*.
619 60:217-227.
620 Volchuk, A., M. Amherdt, M. Ravazzola, B. Brugger, V.M. Rivera, T. Clackson, A. Perrelet, T.H. Sollner,
621 J.E. Rothman, and L. Orci. 2000. Megavesicles implicated in the rapid transport of
622 intracisternal aggregates across the Golgi stack. *Cell*. 102:335-348.
623 Weigel, A.V., C.L. Chang, G. Shtengel, C.S. Xu, D.P. Hoffman, M. Freeman, N. Iyer, J. Aaron, S. Khuon,
624 J. Bogovic, W. Qiu, H.F. Hess, and J. Lippincott-Schwartz. 2021. ER-to-Golgi protein delivery
625 through an interwoven, tubular network extending from ER. *Cell*. 184:2412-2429 e2416.
626 Wessels, E., D. Duijsings, T.K. Niu, S. Neumann, V.M. Oorschot, F. de Lange, K.H. Lanke, J.
627 Klumperman, A. Henke, C.L. Jackson, W.J. Melchers, and F.J. van Kuppeveld. 2006. A viral
628 protein that blocks Arf1-mediated COP-I assembly by inhibiting the guanine nucleotide
629 exchange factor GBF1. *Dev Cell*. 11:191-201.

630

Figure legends

Figure 1

The intra-Golgi transport kinetics for RUSH Reporters in Golgi ministacks. HeLa cells transiently co-expressing individual RUSH reporter and GalT-mCherry were incubated with 33 µM nocodazole for 3 hours. This was followed by a chase with 33 µM nocodazole, 10 µg/ml cycloheximide, and 40 µM biotin for variable time durations (*t*) before fixation and GM130 immunostaining. Except for TNFα-SBP-GFP, which uses Ii-Streptavidin as the ER hook, all RUSH reporters employ signal sequence fused streptavidin-KDEL as their ER hook. Using GLIM, *LQ*s for the RUSH reporters were then calculated and plotted. Each panel has an *LQ* vs. time plot on the left, with *n* (the number of analyzable Golgi ministacks), adj. R^2, y_0, and t_{intra} indicated. On the right side of each panel, the d*LQ*/d*t* vs. time plot represents the first-order derivative of its corresponding *LQ* vs. time plot on the left. ERES/ERGIC ($LQ < -0.25$), *cis* ($-0.25 \leq LQ < 0.25$), medial ($0.25 \leq LQ < 0.75$), *trans*-Golgi ($0.75 \leq LQ < 1.25$), and TGN ($1.25 \leq LQ$) zones were color-shaded. Aside from the one in panel C, all *LQ* vs. time plots are from our previous reports (see Table 1).

Figure 1

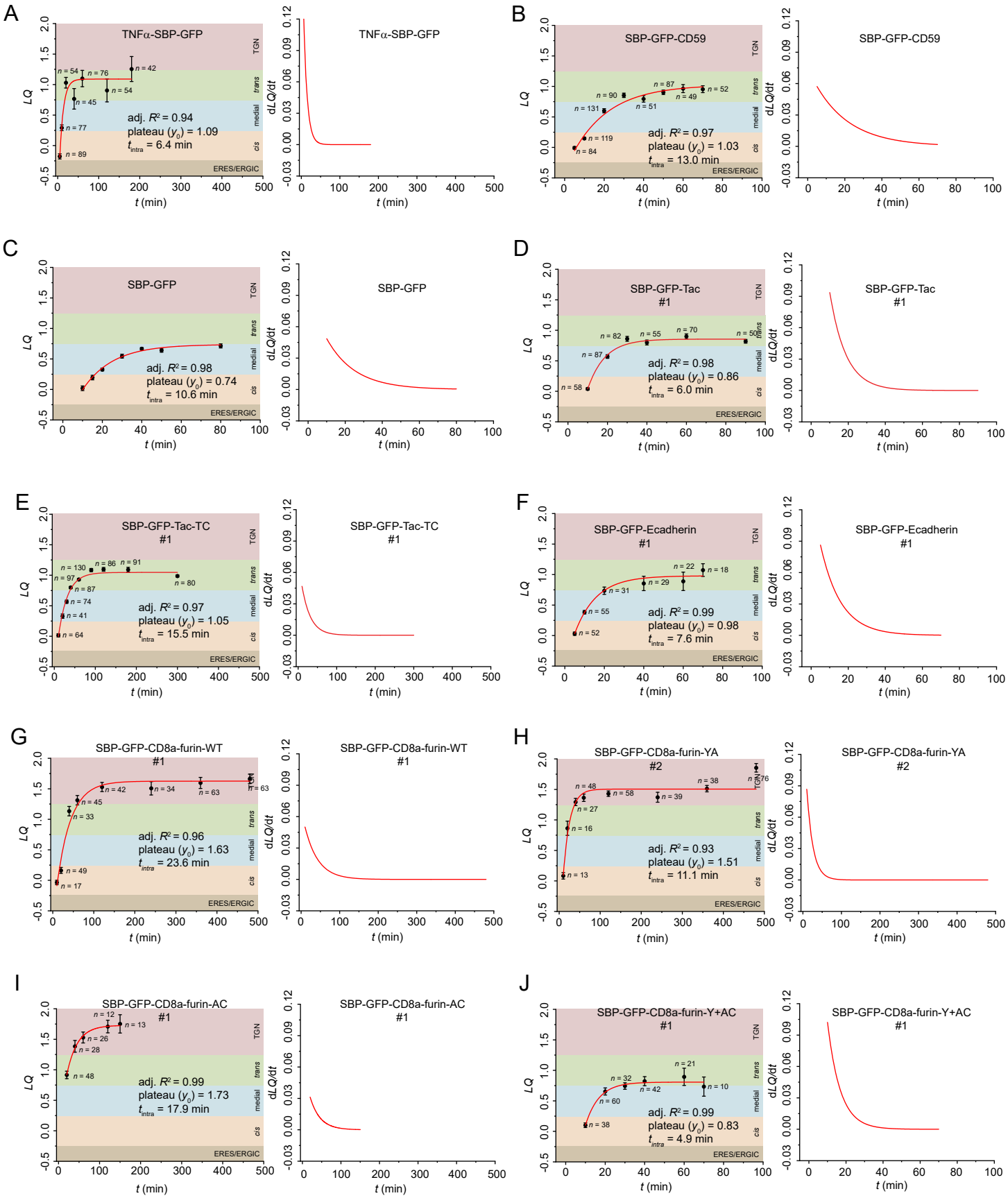
A
TNFα-SBP-GFP
adj. R^2 = 0.94
plateau (y_0) = 1.09
t_{intra} = 6.4 min
B
SBP-GFP-CD59
adj. R^2 = 0.97
plateau (y_0) = 1.03
t_{intra} = 13.0 min
C
SBP-GFP
adj. R^2 = 0.98
plateau (y_0) = 0.74
t_{intra} = 10.6 min
D
SBP-GFP-Tac #1
adj. R^2 = 0.98
plateau (y_0) = 0.86
t_{intra} = 6.0 min
E
SBP-GFP-Tac-TC #1
adj. R^2 = 0.97
plateau (y_0) = 1.05
t_{intra} = 15.5 min
F
SBP-GFP-Ecadherin #1
adj. R^2 = 0.99
plateau (y_0) = 0.98
t_{intra} = 7.6 min
G
SBP-GFP-CD8a-furin-WT #1
adj. R^2 = 0.96
plateau (y_0) = 1.63
t_{intra} = 23.6 min
H
SBP-GFP-CD8a-furin-YA #2
adj. R^2 = 0.93
plateau (y_0) = 1.51
t_{intra} = 11.1 min
I
SBP-GFP-CD8a-furin-AC #1
adj. R^2 = 0.99
plateau (y_0) = 1.73
t_{intra} = 17.9 min
J
SBP-GFP-CD8a-furin-Y+AC #1
adj. R^2 = 0.99
plateau (y_0) = 0.83
t_{intra} = 4.9 min
LQ
dLQ/dt
t (min)
TGN
trans
medial
cis
ERES/ERGIC

Figure 2

Different secretory cargos exhibit distinct intra-Golgi transport velocities within the same cisternae of Golgi ministacks. (A) Plots of d*LQ*/d*t* vs. *LQ* for selected RUSH reporters reveal diverse intra-Golgi transport velocities at the same cisternae. These plots were constructed based on Equation 3, using parameters from Table 1. Different regions within the Golgi — *cis* ($-0.25 \leq LQ < 0.25$), medial ($0.25 \leq LQ < 0.75$), *trans*-Golgi ($0.75 \leq LQ < 1.25$), and TGN ($1.25 \leq LQ$) — are color-shaded for easier identification. To convert d*LQ*/d*t* to nm/min, we multiplied d*LQ*/d*t* by 274 nm per *LQ* unit. A dotted vertical line marks the *LQ* value of 0.40. (B) Modifying the classic cisternal progression model to explain the distinct intra-Golgi transport velocities at the same cisternae. According to this model, Golgi cisternae progress at a constant velocity (v). Direct-continuity-based anterograde transport could accelerate the intra-Golgi transport velocity ($v + \Delta v$), while the COPI-mediated retrograde transport could reduce it ($v - \Delta v$).

Figure 2

A

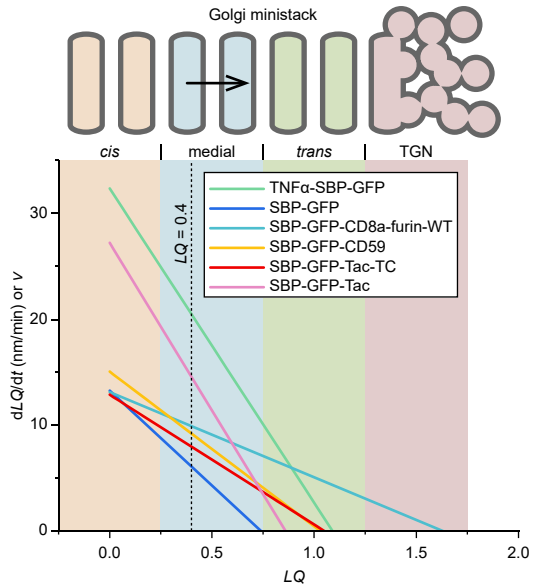
Golgi ministack
cis
medial
trans
TGN
TNFα-SBP-GFP
SBP-GFP
SBP-GFP-CD8a-furin-WT
SBP-GFP-CD59
SBP-GFP-Tac-TC
SBP-GFP-Tac
LQ = 0.4
dLQ/dt (nm/min) or v
LQ
0
10
20
30
0.0
0.5
1.0
1.5
2.0

B

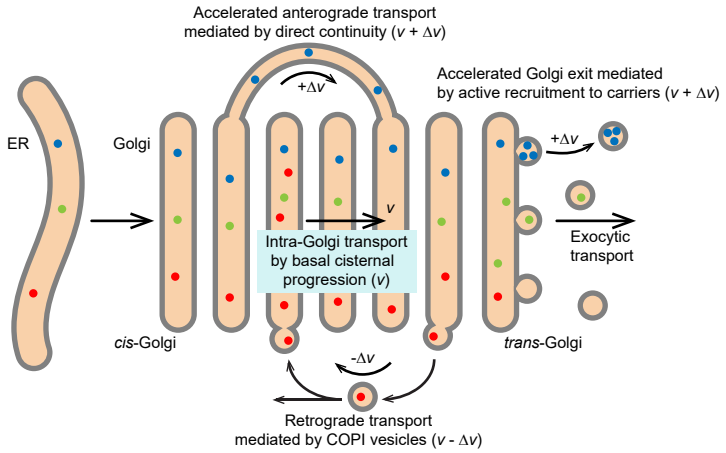
Accelerated anterograde transport
mediated by direct continuity (v + Δv)
+Δv
Accelerated Golgi exit mediated
by active recruitment to carriers (v + Δv)
ER
Golgi
+Δv
v
Intra-Golgi transport
by basal cisternal
progression (v)
Exocytic
transport
cis-Golgi
trans-Golgi
-Δv
Retrograde transport
mediated by COPI vesicles (v - Δv)

Figure 3

GFP-Tac-TC and GFP-CD8a-TC might not have a Golgi retrieval mechanism once exiting the Golgi. (A) Domain organization of GFP-tagged Tac, Tac-TC, CD8a, and CD8a-TC. ss, signal sequence. Mem., membrane. $t_{1/2}$ values are from Table 2 and shown as mean ± SEM. *n*, the number of cells analyzed. (B) The plasma membrane-localized GFP-Tac-TC and GFP-CD8a-TC are not retrieved to the Golgi. HeLa cells transiently expressing indicated GFP-tagged protein were incubated continuously with VHH-anti-GFP-mCherry for 8 h before fixation and immunostaining for the endogenous Golgi marker, GM130. Images were acquired under a wide-field microscope. The internalized VHH-anti-GFP-mCherry has negative Golgi localization for all GFP-tagged proteins except for MGAT2 (arrows), a positive control. The percentage of cells showing the Golgi localization of VHH-anti-GFP-mCherry is labeled at right. *n*, the number of cells analyzed. Scale bar, 10 µm.

Figure 3

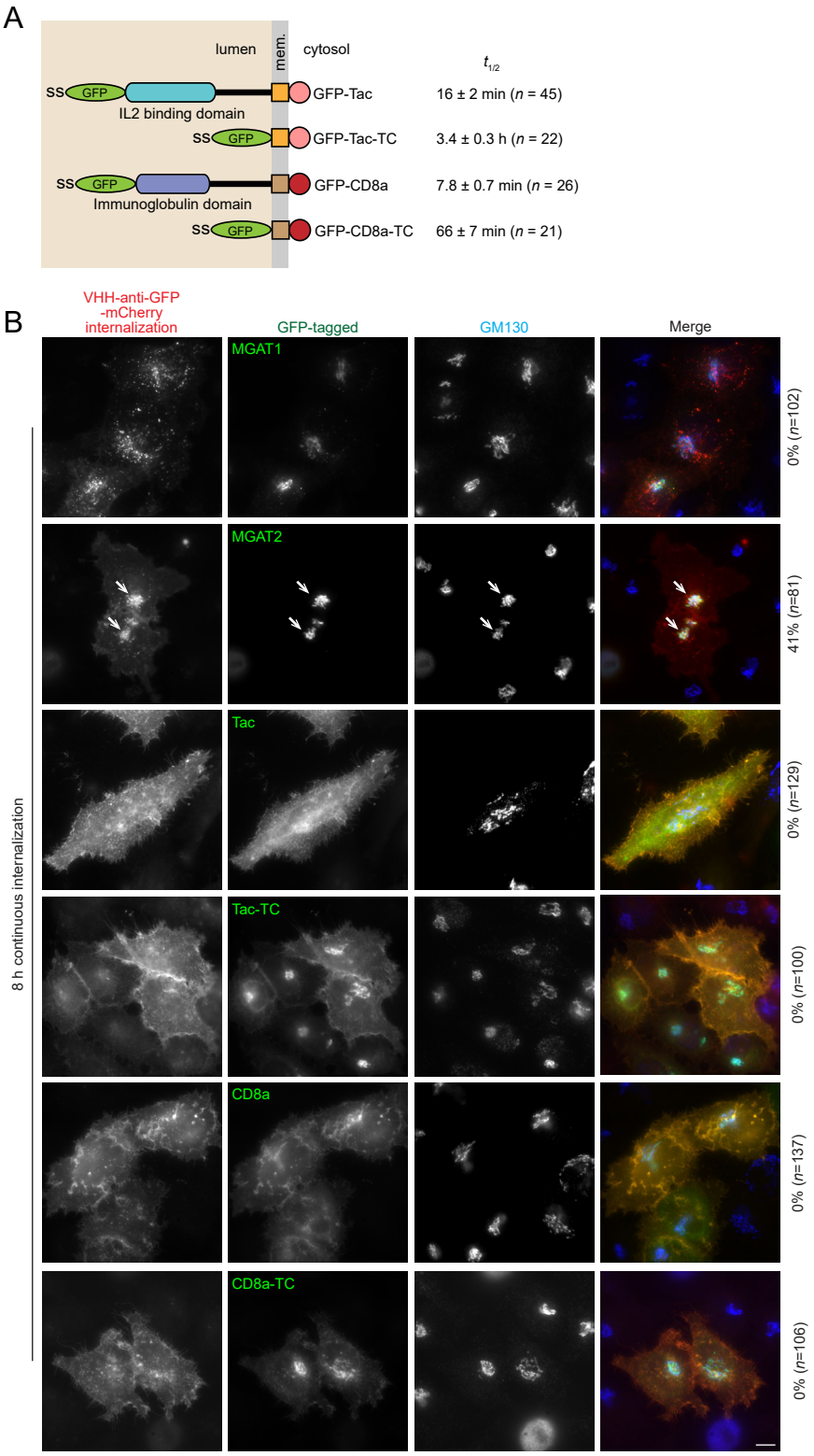
A
lumen
mem.
cytosol
$t_{1/2}$
SS
GFP
IL2 binding domain
GFP-Tac
16 ± 2 min (n = 45)
GFP-Tac-TC
3.4 ± 0.3 h (n = 22)
Immunoglobulin domain
GFP-CD8a
7.8 ± 0.7 min (n = 26)
GFP-CD8a-TC
66 ± 7 min (n = 21)
B
VHH-anti-GFP -mCherry internalization
GFP-tagged
GM130
Merge
8 h continuous internalization
MGAT1
0% (n=102)
MGAT2
41% (n=81)
Tac
0% (n=129)
Tac-TC
0% (n=100)
CD8a
0% (n=137)
CD8a-TC
0% (n=106)

Figure 4

The organization of Golgi ministacks under the BFA treatment. HeLa cells transiently co-expressing GalT-mCherry and indicated GFP or CD8a-tagged Golgi proteins were incubated with 33 µM nocodazole for 3 hours. This was followed by additional treatment with 33 µM nocodazole and 1 µM BFA for variable durations before fixation. Endogenous GS15 and TGN46 were immunostained. *LQ*s of different Golgi proteins were then determined using GLIM. The dotted lines represent *LQ*s for GM130 (*LQ* = 0.00) and GalT-mCherry (*LQ* = 1.00). The total number of analyzed Golgi ministacks is denoted by '*n*'.

Figure 4

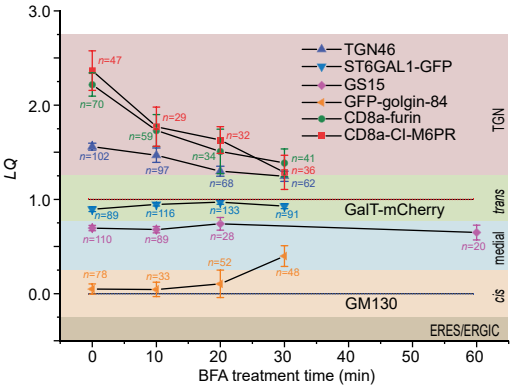
3.0
2.0
1.0
0.0
LQ
TGN46
ST6GAL1-GFP
GS15
GFP-golgin-84
CD8a-furin
CD8a-CI-M6PR
TGN
trans
medial
cis
GalT-mCherry
GM130
ERES/ERGIC
n=47
n=70
n=29
n=59
n=32
n=102
n=97
n=34
n=68
n=41
n=36
n=62
n=89
n=116
n=133
n=91
n=110
n=89
n=28
n=20
n=78
n=33
n=52
n=48
0
10
20
30
40
50
60
BFA treatment time (min)

Supplementary information

Supplementary Figure 1

Additional intra-Golgi transport kinetics of RUSH reporters. All *LQ* vs. time plots, except those in panels (A-C), are from our previous reports (see Table I). See Figure 1's legend for details.

Supplementary Figure 1

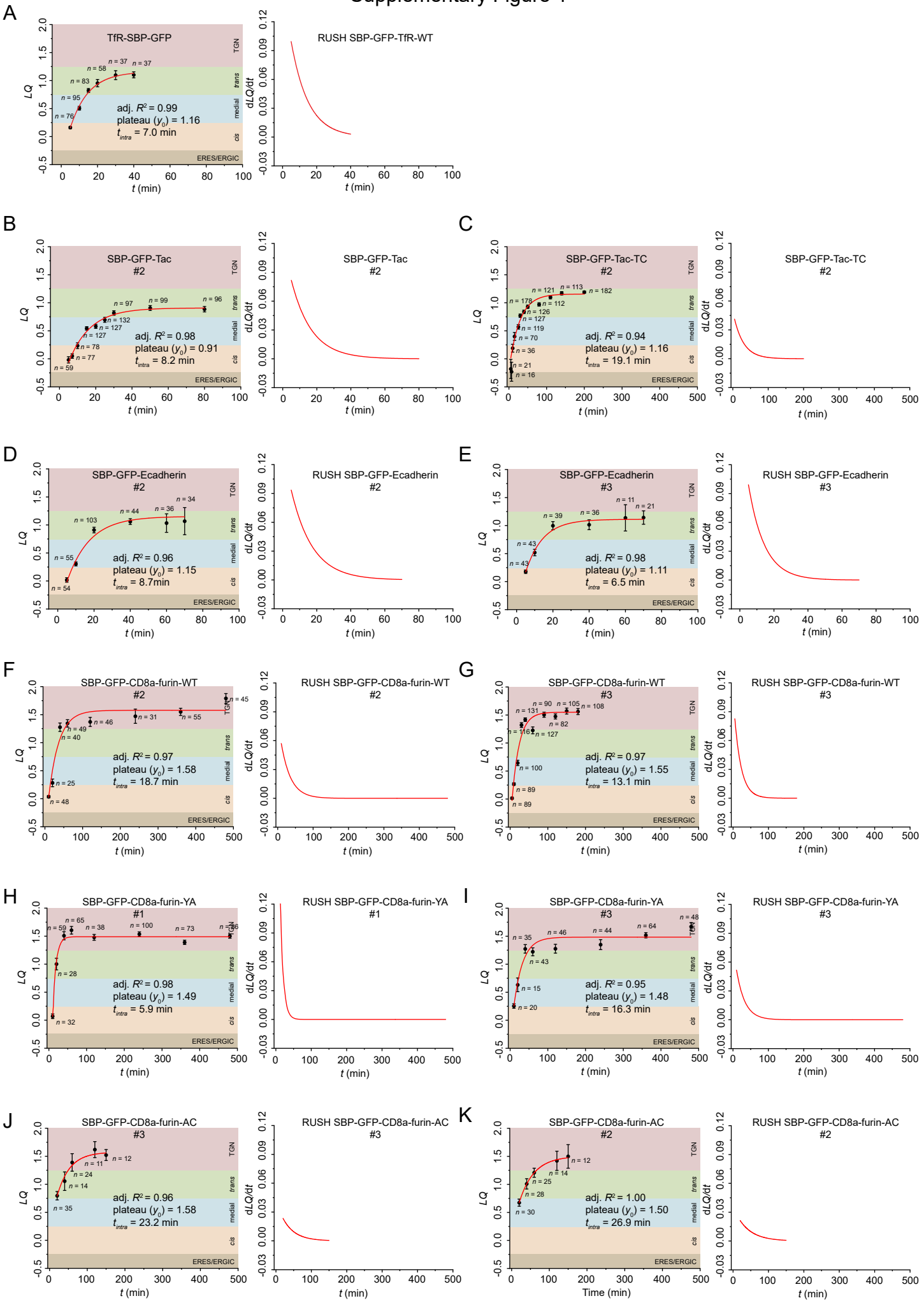

Supplementary Figure 1

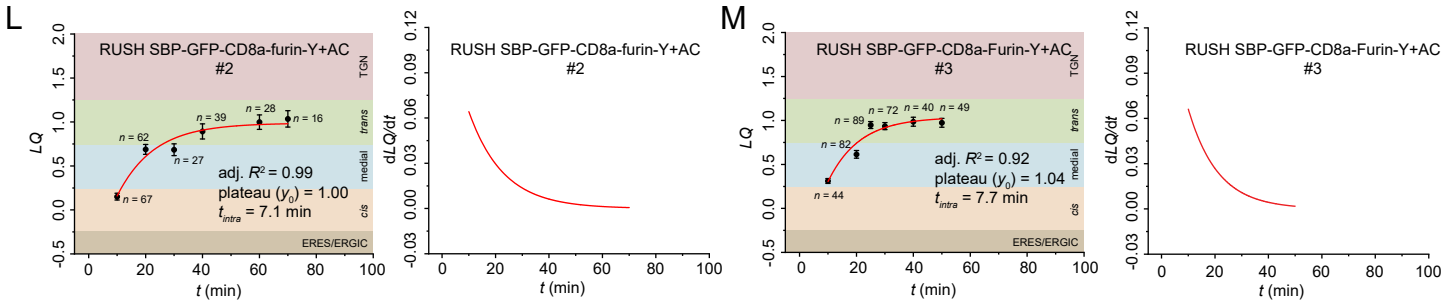

Supplementary Figure 2

Acquiring Golgi residence times of RUSH SBP-GFP-CD59 and GFP-CD8a-TC. (A) HeLa cells were transiently transfected to co-express RUSH SBP-GFP-CD59 and GalT-mCherry. Cells were incubated with 40 µM biotin and 10 µg/ml cycloheximide at 20 °C to accumulate the RUSH reporter in the Golgi before live-cell imaging under a wide-field microscope at 37 °C. Only RUSH SBP-GFP-CD59 images are shown. (B) HeLa cells transiently co-expressing GFP-CD8a-TC and GalT-mCherry were treated with cycloheximide and imaged live under a wide-field microscope. Only GFP-CD8a-TC images are shown. In both (A) and (B), the total fluorescence intensity within the Golgi was quantified, normalized, and plotted against the time. Each intensity series was fitted to the first-order exponential function to calculate $t_{1/2}$. Grey and red indicate individual and averaged time series, respectively. CHX, cycloheximide. Error bar, mean ± stand error of the mean. *n*, the number of quantified cells. Scale bar, 10 µm.

Supplementary Figure 2

A

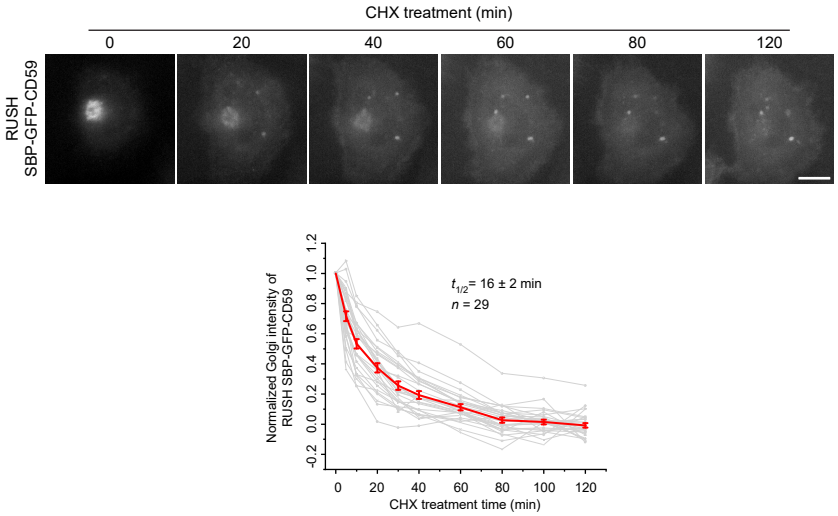

B

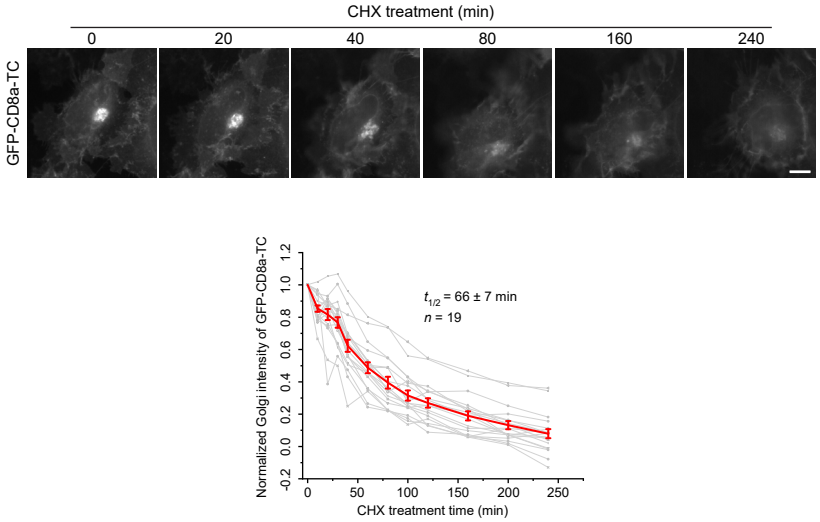

Supplementary Figure 3

The localization of Arf1 and golgin-84 under the treatment of nocodazole and BFA. (A) HeLa cells transiently expressing Arf1-GFP and ST6GAL1-DMyc were treated with 33 μM nocodazole for 3 hours. This was followed by additional treatment with 33 μM nocodazole and 1 μM BFA for 5 min before fixation and immunostaining of Myc-tag and giantin. Images were acquired by Airyscan microscopy. (B) HeLa cells transiently expressing GalT-mCherry and GFP-golgin-84 were treated with 33 μM nocodazole for 3 hours. This was followed by additional treatment with 33 μM nocodazole and 1 μM BFA for 30 min before fixation and immunostaining for GM130. Images were acquired by wide-field microscopy. Scale bar, 10 μm.

Supplementary Figure 3

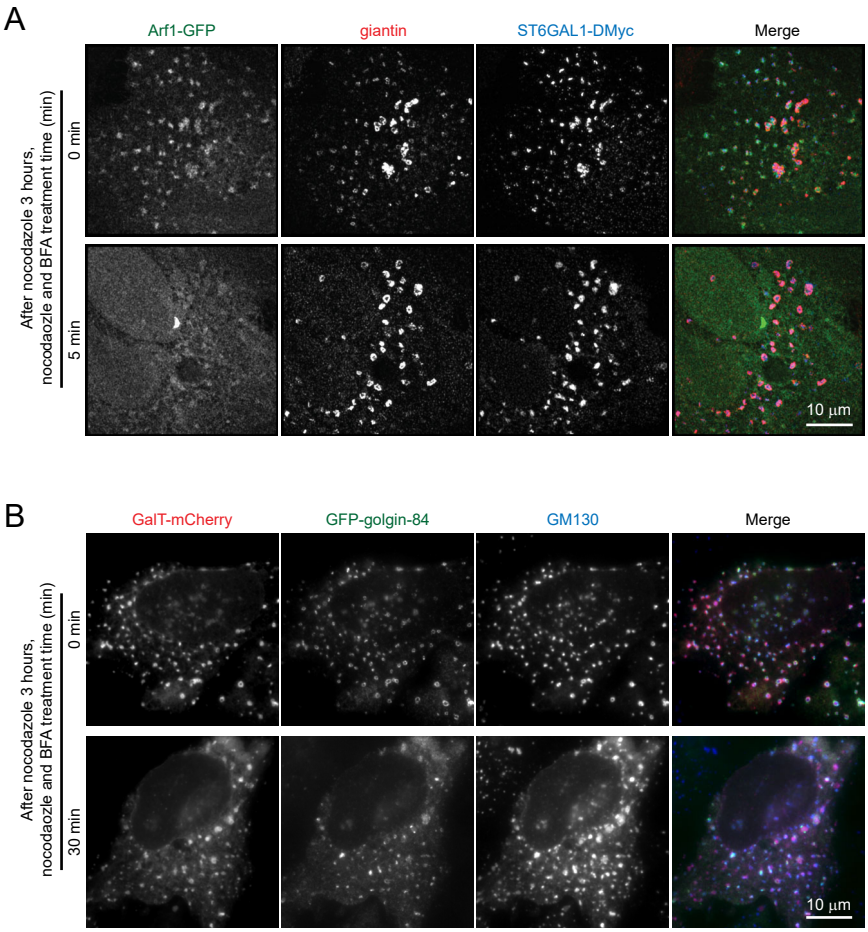

Supplementary File 1

LQ data employed in plots presented in Figure 1, Figure 4, and Supplementary Figure 1. *n*, the number of quantified cells. SEM, standard error of the mean.

Supplementary File 1

Fig. 1

A. SBP-TNFα-GFP

Chase time (min)	*n*	*LQ*	*SEM*
5	89	-0.18	0.04
10	77	0.29	0.05
20	54	1.03	0.09
40	45	0.77	0.17
60	76	1.10	0.13
120	54	0.90	0.19
180	42	1.25	0.21

B. SBP-GFP-CD59

5	84	-0.01	0.02
10	119	0.15	0.02
20	131	0.60	0.03
30	90	0.85	0.04
40	51	0.80	0.05
50	87	0.90	0.04
60	49	0.96	0.07
70	52	0.95	0.06

C. SBP-GFP

10	67	0.02	0.04
15	84	0.19	0.04
20	124	0.33	0.02
30	138	0.55	0.03
40	207	0.67	0.02
50	105	0.64	0.03
80	82	0.71	0.03

D. SBP-GFP-Tac #1

10	58	0.04	0.02
20	87	0.57	0.03
30	82	0.86	0.04
40	55	0.80	0.04
60	70	0.90	0.04
90	50	0.82	0.03

E. SBP-GFP-Tac-TC #1

10	64	0.02	0.03
20	41	0.33	0.04
30	74	0.57	0.03
40	87	0.80	0.02
60	97	0.93	0.02
90	130	1.08	0.03
120	86	1.10	0.03
180	91	1.09	0.04
300	80	0.99	0.02

F. SBP-GFP-Ecadherin #1

5	52	0.03	0.03
10	55	0.38	0.03
20	31	0.74	0.06
40	29	0.85	0.12
60	22	0.89	0.15
70	18	1.07	0.10

10	17	-0.03	0.04
20	49	0.16	0.05

G. SBP-GFP-CD8a-furin-WT #1

40	33	1.13	0.08
60	45	1.31	0.08
120	42	1.53	0.07
240	34	1.51	0.11
360	63	1.60	0.09
480	63	1.66	0.08

H. SBP-GFP-CD8a-furin-YA #2

10	13	0.08	0.05
20	16	0.86	0.12
40	27	1.29	0.06
60	48	1.36	0.06
120	58	1.43	0.04
240	39	1.37	0.08
360	38	1.51	0.05
480	76	1.85	0.07

I. SBP-GFP-CD8a-furin-AC #1

20	48	0.92	0.06
40	28	1.38	0.10
60	26	1.53	0.09
120	12	1.71	0.10
150	13	1.75	0.15

J. SBP-GFP-CD8a-furin-Y+AC #1

10	38	0.10	0.04
20	60	0.65	0.06
30	32	0.74	0.05
40	42	0.82	0.07
60	21	0.89	0.14
70	10	0.73	0.16

Fig. 4

	BFA treatment time (min)	*n*	*LQ*	*SEM*
TGN46	0	102	1.56	0.04
	10	97	1.47	0.08
	20	68	1.30	0.05
	30	62	1.25	0.05
ST6GAL1-moxGFP	0	89	0.90	0.03
	10	116	0.95	0.02
	20	133	0.97	0.02
	30	91	0.93	0.03
GS15	0	110	0.70	0.03
	10	89	0.68	0.03
	20	28	0.74	0.07
	60	20	0.65	0.08
GFP-golgin-84	0	78	0.05	0.05
	10	33	0.04	0.08
	20	52	0.10	0.15
	30	48	0.40	0.11
CD8a-furin	0	70	2.22	0.12
	10	59	1.73	0.17
	20	34	1.51	0.24
	30	41	1.39	0.15
CD8a-CI-M6PR	0	47	2.37	0.21
	10	29	1.77	0.21
	20	32	1.63	0.14
	30	36	1.29	0.18

Fig. S1

A. SBP-GFP-TfR-WT

Chase time (min)	*n*	*LQ*	*SEM*
5	76	0.16	0.02
10	95	0.51	0.03
15	83	0.82	0.03
20	58	0.95	0.06
30	37	1.10	0.08
40	37	1.10	0.05

B. SBP-GFP-Tac #2

5	59	-0.02	0.06
7	77	0.05	0.04
10	78	0.23	0.05
15	127	0.54	0.03
20	127	0.58	0.04
25	132	0.70	0.04
30	97	0.82	0.04
50	99	0.91	0.04
80	96	0.89	0.05

C. SBP-GFP-Tac-TC #2

5	21	-0.18	0.17
7	16	-0.23	0.17
10	36	0.19	0.07
15	70	0.40	0.07
25	119	0.69	0.09
30	127	0.77	0.03
40	126	0.84	0.03
50	178	0.93	0.03
80	112	0.99	0.02
110	121	1.11	0.03
140	113	1.18	0.03
200	182	1.19	0.02

D. SBP-GFP-Ecadherin #2

5	54	0.02	0.04
10	55	0.31	0.04
20	103	0.91	0.05
40	44	1.06	0.05
60	36	1.03	0.17
70	34	1.07	0.24

E. SBP-GFP-Ecadherin #3

5	43	0.18	0.03
10	43	0.52	0.06
20	39	1.00	0.07
40	36	1.01	0.09
60	11	1.14	0.23
70	21	1.14	0.12

F. SBP-GFP-CD8a-furin-WT #2

10	48	0.04	0.02
20	25	0.28	0.07
40	40	1.28	0.08
60	49	1.34	0.07

F. SBP-GFP-CD8a-furin-WT #2

120	46	1.37	0.08
240	31	1.47	0.13
360	55	1.55	0.06
480	45	1.79	0.09

G. SBP-GFP-CD8a-furin-WT #3

5	89	0.02	0.02
10	89	0.27	0.02
20	100	0.64	0.05
30	116	1.32	0.04
40	131	1.42	0.03
60	127	1.23	0.06
90	90	1.51	0.05
120	82	1.47	0.05
150	105	1.57	0.05
180	108	1.56	0.05

H. SBP-GFP-CD8a-furin-YA #1

10	32	0.07	0.04
20	28	1.00	0.10
40	59	1.51	0.07
60	65	1.61	0.07
120	38	1.48	0.05
240	100	1.54	0.04
360	73	1.39	0.04
480	86	1.50	0.04

I. SBP-GFP-CD8a-furin-YA #3

10	20	0.25	0.04
20	15	0.63	0.12
40	35	1.27	0.08
60	43	1.22	0.07
120	46	1.28	0.08
240	44	1.35	0.09
360	64	1.52	0.05
480	48	1.67	0.07

J. SBP-GFP-CD8a-furin-AC #3

20	35	0.80	0.07
40	14	1.06	0.17
60	24	1.39	0.16
120	11	1.62	0.14
150	12	1.52	0.10

K. SBP-GFP-CD8a-furin-AC #2

20	30	0.67	0.06
40	28	1.01	0.09
60	25	1.21	0.08
120	14	1.42	0.17
150	12	1.50	0.21

L. SBP-GFP-CD8a-furin-Y+AC #2

10	67	0.15	0.04
20	62	0.69	0.06
30	27	0.68	0.07
40	39	0.89	0.09

60	28	1.00	0.08
70	16	1.04	0.09

M. SBP-GFP-CD8a-furin-Y+AC #3

10	44	0.31	0.03
20	82	0.62	0.04
25	89	0.95	0.04
30	72	0.94	0.04
40	40	0.99	0.05
50	49	0.97	0.05